National Metrology Institute VTT MIKES
October 31, 2026

Frequency evaluation of MIKES AHM3 by MIKES-Sr+1 for the period MJD 61309 to 61344

The frequency of the hydrogen maser (HM) MIKES AHM3 (1404189) was evaluated during the 35-day period MJD 61309 to 61344 using the $^{88}Sr^{+}$ optical single-ion frequency standard MIKES-Sr+1 (1784101) and an optical frequency comb. The $^{88}Sr^{+}$ standard operated for 91.5% of the period. The evaluation is based on the 2025 recommended frequency for the $5s\,^2S_{1/2} \rightarrow 4d\,^2D_{5/2}$ transition in $^{88}Sr^{+}$, 444 779 044 095 485.347 Hz, with a fractional uncertainty of 1.7×10^{-16} [1]. The results of the evaluation are given in Table 1. The operation and uncertainty evaluation of MIKES-Sr+1 are described in [2] and summarized below.

Table 1: Results of the evaluation of AHM3 by MIKES-Sr+1.

Period of estimation	y(AHM3/Sr+1) $/10^{-15}$	u_A $/10^{-15}$	u_B $/10^{-15}$	$u_{A/Lab}$ $/10^{-15}$	$u_{B/Lab}$ $/10^{-15}$	u_{Srep} $/10^{-15}$	Uptime %
61309–61344	51.64	0.0015	0.0026	0.12	0.020	0.17	91.5

1 Measurement configuration

The measurement configuration is schematically shown in Fig. 1. The clock laser is a 1348 nm external-cavity diode laser (ECDL). In contrast to the work in [2], it is now stabilized to an 18 cm vertical ultra-low-expansion (ULE) glass cavity. The light to the ion is frequency doubled to 674 nm. The light to the ion and the frequency comb is de-drifted by an acousto-optic modulator (AOM, frequency f_{drift}) based on feedback from the ion. Using another AOM (frequency f_{Zeeman}), independent servo loops track six Zeeman components of the clock transition, whose mean is free from linear Zeeman shift and tensor shifts. The fibre frequency comb is optically locked to the clock laser. The frequency ratio between the HM and MIKES-Sr+1 is determined from the

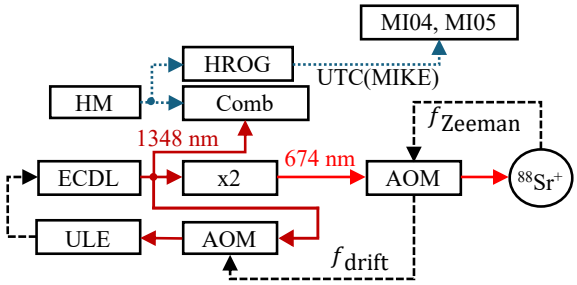


Figure 1: Clock-laser setup and frequency chain to the $^{88}Sr^{+}$ ion, frequency comb, hydrogen maser (HM), and geodetic GNSS receivers MI04 and MI05 for time transfer. HROG—high resolution offset generator. Solid (dotted) lines indicate optical (rf) signals, while dashed lines indicate feedback loops for Pound-Drever-Hall locking (left), drift compensation of the cavity (f_{drift}, middle), and tracking the Zeeman components of the clock transition (f_{Zeeman}, right). AOMs for fiber noise cancellation are not shown.

AOM frequencies, the in-loop beat note between the clock laser and the comb, and from the comb repetition rate and carrier offset frequency measured against the HM. For details, see [2].

2 MIKES-Sr+1 evaluation

A detailed uncertainty evaluation is presented in [2]. The statistical uncertainty $u_{\mathrm{A},i}$ of a particular measurement i is estimated from a $\tau^{-1/2}$ fit to the clock self-comparison instability evaluated at the total measurement time τ_i (including valid data only). The instability varies with the probe time (and dead time). During this evaluation period, it was on average $2.5{\times}10^{-15}\tau^{-1/2}$. The total u_{A} of the period is determined as $u_{\mathrm{A}} = (\sum_i w_i^2 u_{\mathrm{A},i}^2)^{1/2}$, where the weights are proportional to the duration of the individual measurements, $w_i = \tau_i/(\sum_i \tau_i)$.

Several systematic frequency shifts are evaluated dynamically. Several systematic uncertainty contributions j also depend on parameters such as the probe time (light shifts, thermal motion shifts via the ion heating rate), the Zeeman AOM rf power (AOM chirp), the trap drive voltage (blackbody radiation shift), and the electric quadrupole shift and excess micromotion measured during a clock run. Each uncertainty contribution is assumed to be fully correlated throughout the evaluation period so that its weighted mean is $u_{\mathrm{B},j} = \sum_i w_i u_{\mathrm{B},i,j}$. The total systematic uncertainty is then evaluated as $u_{\mathrm{B}} = (\sum_j u_{\mathrm{B},j}^2)^{1/2}$. An uncertainty budget for the evaluation period is shown in Table 2.

The relativistic redshift given in [2] and used for TAI calibration up to 2026-03 is in the zero-tide system. Starting 2026-04, the mean-tide potential evaluated at our latitude of 60.18° is included, which increases the shift value by 1.35×10^{-17}. Due to the Fennoscandian land uplift (postglacial rebound), the height of the clock relative to the reference potential $W_0 = 62\,636\,856.00\,\mathrm{m}^2/\mathrm{s}^2$ increases by 3.8 mm/year. For simplicity, this evaluation has been automated based on the mean epoch of a particular measurement. The uncertainty of the (nearly) static redshift is 2.4×10^{-18} and the uncertainty from not considering the explicit time dependence of the tide potential is estimated to be 0.7×10^{-18} for a 35-day period, resulting in a total redshift uncertainty of 2.5×10^{-18}.

3 Frequency comparison

The measured maser frequency and the uptime of MIKES-Sr+1 for the evaluation period are shown in Fig. 2. **On MJD 61326, an interruption in the district heating caused a transient in the HM laboratory temperature and thus also in the HM frequency. The transient behavior lasted about 14 h (MJD 61326.85–61327.45) and was tracked by the optical clock with an uptime of 99.5%.** The statistical uncertainty $u_{\mathrm{A/Lab}}$ includes the uncertainty due to the dead time of MIKES-Sr+1 (DTU). The DTU consists of a deterministic part due to the HM drift and a stochastic part. The frequency in the middle of the evaluation period is obtained by correcting the measured mean frequency using the drift and the offset between the middle point and the barycenter of the data. The drift was estimated from a linear fit over the evaluation period, **excluding the anomaly**. The noise model for the maser is given in Table 3. As in [4], the bump in the power spectral density, caused by quasi-periodic frequency jumps, is described by a Lorentzian peak. The extrapolation uncertainty is evaluated using the Fourier transform method [5]. **The extrapolation error from the 0.05% missing data during the anomaly was estimated by interpolating the missing points, summing the differences between the interpolated points and the linear fit, and dividing the sum by the total number of valid points. The result, 1.5×10^{-18}, was added in quadrature to the normal extrapolation uncertainty, but its contribution is negligible.**

The UTC(k)-HM data is submitted to the BIPM with a resolution of 0.1 ns. The standard deviation of the rectangular distribution of rounding errors is $u_{x,\mathrm{round}} = 0.1/\sqrt{12}$ ns. When evaluating the mean frequency over a period of duration T, this gives rise to a fractional uncertainty $u_{y,\mathrm{round}} = \sqrt{2}u_{x,\mathrm{round}}/T \approx 4.7 \times 10^{-16}/(T/\mathrm{d})$. The statistical uncertainty of the measurement itself

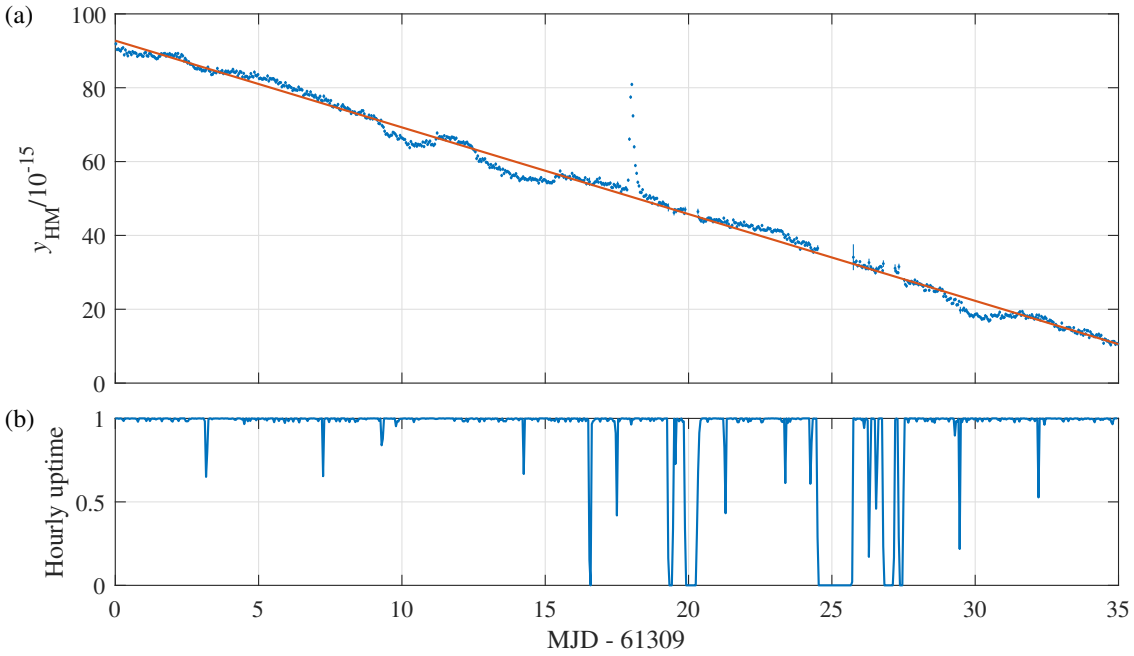


Figure 2: (a) Maser fractional frequency as measured against MIKES-Sr+1 in 1 h wall-clock bins (dots). The error bars are the Allan deviation at an integration time corresponding to the number of valid 1 S/s points in the bin and the line is a linear fit. (b) Hourly uptime of MIKES-Sr+1 over the evaluation period (total uptime 91.5%).

is estimated to be $u_{y,\mathrm{meas}} \approx 2.8 \times 10^{-16}/(T/\mathrm{d})$, including the 1 PPS signal distribution. The total UTC(k)-HM uncertainty is included in $u_{\mathrm{A/Lab}}$.

An upper limit of 2×10^{-17} for the systematic uncertainty $u_{\mathrm{B/Lab}}$ was estimated in a comparison between two frequency combs with independent rf distribution [2]. The corresponding statistical uncertainty was found to be negligible compared to $u_{\mathrm{B/Lab}}$ for relevant measurement times and is not included in $u_{\mathrm{A/Lab}}$. The $u_{\mathrm{A/Lab}}$ and $u_{\mathrm{B/Lab}}$ contributions are summarized in Table 4.

References

[1] BIPM, Recommended values of standard frequencies.

[2] T. Lindvall *et al.*, $^{88}Sr^{+}$ optical clock with 7.9×10^{-19} systematic uncertainty and its absolute frequency with 9.8×10^{-17} uncertainty, Phys. Rev. Applied **24**, 044082 (2025).

[3] T. Lindvall *et al.*, Measurement of the Differential Static Scalar Polarizability of the $^{88}Sr^{+}$ Clock Transition, Phys. Rev. Lett. **135**, 043402 (2025).

[4] T. Lindvall *et al.*, Coordinated international comparisons between optical clocks connected via fiber and satellite links, Optica **12**, 843–852 (2025).

[5] S. T. Dawkins *et al.*, Considerations on the measurement of the stability of oscillators with frequency counters, IEEE Trans. Ultrason., Ferroelectr., Freq. Control **54**, 918 (2007).

Table 2: Uncertainty budget for MIKES-Sr+1 for the reported evaluation period (10^{-18}).

Contribution	Shift	Uncertainty
Blackbody radiation (BBR) E1 shift	522.65	
BBR field		0.36
Differential polarizability $\Delta\alpha_0^{\dagger}$		0.22
Dynamic correction η		0.089
BBR M1 shift	−0.0101	0.0002
Collisional shift	0.00	0.22
Thermal motion shifts	−1.24	0.32
Electrical quadrupole shift	0.000	0.032
Excess micromotion shifts	0.000	0.009
Tensor Stark shift	0.000	0.002
674 nm E1 ac Stark shift	0.005	0.010
674 nm E2 ac Stark shift	0.000	0.007
Quadratic Zeeman shift, static field	0.188	0.004
AOM chirp	0.00	0.23
Servo errors	0.00	0.10
First-order Doppler shifts	0.00	0.50
Total, Sr^+	521.59	0.81
Gravitational redshift	817.3	2.5
Total	1338.9	2.6

† $\Delta\alpha_0 = -4.8314(20) \times 10^{-40}\mathrm{Jm}^2/\mathrm{V}^2$ [3].

Table 3: Maser noise coefficients for the one-sided fractional-frequency power-spectral-density (PSD) model, $S_y(f) = h_2 f^2 + h_0 + h_{-1}/f + A/[1 + (f - f_0)^2/\delta f^2]$.

White phase noise	h_2	2.8×10^{-24}	Hz^{-3}
Flicker phase noise	h_1	1.5×10^{-26}	Hz^{-2}
White frequency noise	h_0	1.3×10^{-27}	Hz^{-1}
Flicker frequency noise	h_{-1}	7.2×10^{-33}	1
Lorentzian peak	A	6.5×10^{-24}	Hz^{-1}
	f_0	5.0×10^{-8}	Hz
	δf	5.5×10^{-7}	Hz

Table 4: Contributions to $u_{\mathrm{A/Lab}}$ and $u_{\mathrm{B/Lab}}$.

Contribution	Uncertainty/10^{-15}
Extrapolation (stochastic)	0.11
Extrapolation (drift)	0.0010
UTC(MIKE)-HM measurement and rounding	0.016
$u_{\mathrm{A/Lab}}$ total	0.12
rf distribution/synthesis	0.020
$u_{\mathrm{B/Lab}}$ total	0.020